

# Higgs Self-Coupling Measurements at a 100 TeV Hadron Collider

Alan J. Barr,<sup>1</sup> Matthew J. Dolan,<sup>2</sup> Christoph Englert,<sup>3</sup> Danilo Enoque Ferreira de Lima,<sup>3,4</sup> and Michael Spannowsky<sup>4</sup>

<sup>1</sup>*Denys Wilkinson Building, Department of Physics,  
Oxford, OX1 3RH, UK*

<sup>2</sup>*Theory Group, SLAC National Accelerator Laboratory,  
Menlo Park, CA 94025, USA*

<sup>3</sup>*SUPA, School of Physics and Astronomy, University of Glasgow,  
Glasgow, G12 8QQ, UK*

<sup>4</sup>*Institute for Particle Physics Phenomenology, Department of Physics,  
Durham University, DH1 3LE, UK*

An important physics goal of a possible next-generation high-energy hadron collider will be precision characterisation of the Higgs sector and electroweak symmetry breaking. A crucial part of understanding the nature of electroweak symmetry breaking is measuring the Higgs self-interactions. We study diHiggs production in proton-proton collisions at 100 TeV centre of mass energy in order to estimate the sensitivity such a machine would have to variations in the trilinear Higgs coupling around the Standard Model expectation. We focus on the  $b\bar{b}\gamma\gamma$  final state, including possible enhancements in sensitivity by exploiting diHiggs recoils against a hard jet. We find that it should be possible to measure the trilinear self-coupling with 40% accuracy given 3/ab and 12% with 30/ab of data.

## I. INTRODUCTION

The discovery of the Higgs boson [1] at the Large Hadron Collider (LHC) [2] has led to an extensive experimental and theoretical effort to measure and constrain its properties in order to understand in detail the mechanism of electroweak symmetry breaking (EWSB) [3]. A crucial diagnostic in this process is the measurement of the Higgs self-couplings, which directly probe the higher order structure of the Higgs potential and BSM effects [4–6]. While measurement of the quartic Higgs coupling seems unlikely to be possible at any realistic future hadron collider [7], constraints can be set on the Higgs trilinear coupling  $\lambda$  by studying diHiggs production [8]. In the Standard Model (SM) the coupling  $\lambda$  can be expressed in terms of the fundamental SM Lagrangian parameters

$$V(H^\dagger H) = \mu^2 H^\dagger H + \eta(H^\dagger H)^2 \\ \longrightarrow \frac{1}{2}m_h^2 h^2 + \sqrt{\frac{\eta}{2}}m_h h^3 + \frac{\eta}{4}h^4 \quad (1)$$

where we have expanded the potential around the Higgs vacuum expectation value (vev), such that  $\lambda_{\text{SM}} = m_h \sqrt{\eta/2}$ .

Research into diHiggs phenomenology has undergone a renaissance since the Higgs discovery at the LHC. Well studied final states in the gluon fusion production mode now include  $b\bar{b}\tau\tau$  [9–11],  $b\bar{b}WW$  [10, 12] and  $b\bar{b}b\bar{b}$  [9, 10, 13]. There has also been significant work on the vector boson fusion (VBF) [14] and  $t\bar{t}hh$  [15, 16] production mechanisms. However, due to it being the dominant production mechanism we focus exclusively on gluon fusion in this article.

Early work on measuring Higgs trilinears at the LHC includes [17], which suggested the  $b\bar{b}\gamma\gamma$  final state as

a promising possibility. While recent studies by theoreticians generally agree with the results of that article [18, 19], evaluations from the ATLAS [20] and CMS collaborations [21] find that diHiggs production can be measured with considerably lower significance than previously quoted (1.3 and 2  $\sigma$  respectively after 3000/fb), corresponding in the ATLAS analysis to an allowed range of  $8.7 \geq \lambda/\lambda_{\text{SM}} \geq -1.3$  for the Higgs trilinear coupling. This discrepancy between theorists and experimentalists simulations is due to the treatment of backgrounds which are due to fakes: either light jets faking photons or light jets faking  $b$ -jets. A reliable estimate of the fake rate for various reconstructed physics objects is thus a crucial component of any analysis in this channel.

Results from other channels suggest a measurement of the Higgs trilinear at the level of 30–50% may be possible at the LHC [22] using a combination of the above channels and ratios of cross-sections. The proposed International Linear Collider could improve on such a measurement if operated with a centre of mass energy of 1 TeV, in which case an estimated ultimate precision of 13% could be achieved [23, 24]. However, identifying the possible deviations in Higgs self-couplings due to BSM physics may require a measurement at greater than even this accuracy [24, 25].

The discovery of new physics and a complete understanding of electroweak symmetry breaking may therefore require a new high energy hadron collider [26]. A study of the ability of such a collider to constrain the Higgs trilinear couplings was undertaken as part of the Snowmass process [19, 24]. While this study focussed on the  $b\bar{b}\gamma\gamma$  channel, it did not include any of the dominant backgrounds due to fakes.

In this article we therefore comprehensively analyse the process

$$pp \rightarrow hh + X \rightarrow (b + \bar{b}) + (\gamma + \gamma) + X \quad (2)$$

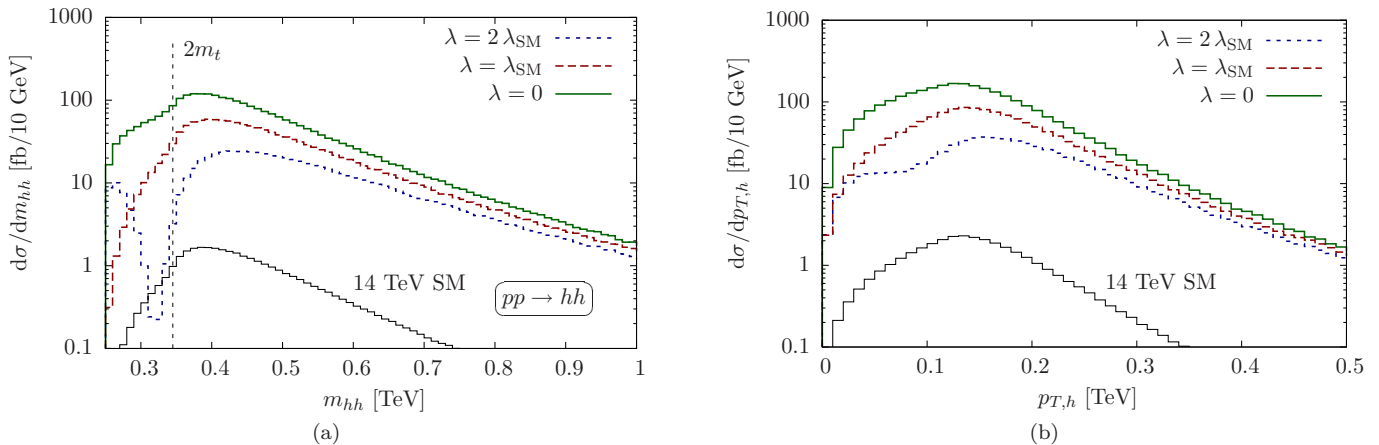


FIG. 1: Leading-order parton level distributions (including flat NLO normalisation  $K$  factors) of the diHiggs invariant mass  $m_{hh}$  and transverse momentum  $p_{T,h}$  for  $pp \rightarrow hh$  at  $\sqrt{s} = 100$  TeV for  $\lambda = 0, \lambda_{\text{SM}}$  and  $2\lambda_{\text{SM}}$ , shown with the  $\lambda/\lambda_{\text{SM}} = 1$  case for  $\sqrt{s} = 14$  TeV for comparison.

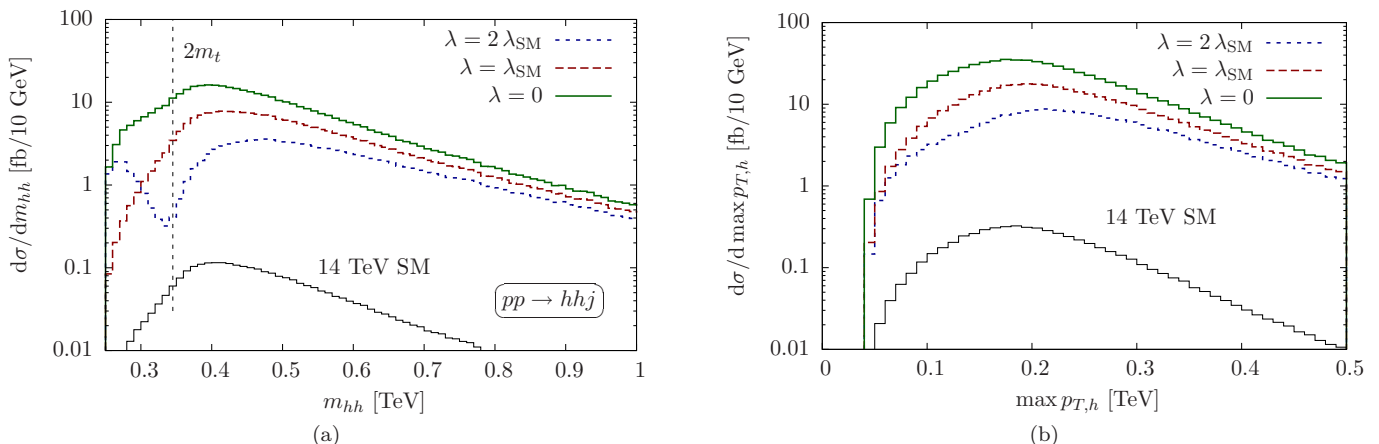


FIG. 2: Leading-order parton level distributions of the diHiggs invariant mass  $m_{hh}$  and maximum transverse momentum  $\max p_{T,h}$  for  $pp \rightarrow hhj$  at  $\sqrt{s} = 100$  TeV for  $p_{T,j} \geq 80$  GeV and  $|\eta_j| \leq 4.5$ , for  $\lambda = 0, \lambda_{\text{SM}}$  and  $2\lambda_{\text{SM}}$ . We also include the  $\lambda/\lambda_{\text{SM}} = 1$  case for  $\sqrt{s} = 14$  TeV for comparison.

at  $\sqrt{s} = 100$  TeV in order to provide a reliable estimate of the sensitivity which a very high energy hadron collider would have to variations in the trilinear Higgs coupling. We also consider the related same process accompanied by a high transverse momentum jet, which, as argued in [10], accesses new regions of phase space as well as offering a powerful means to further suppress background processes at the LHC.

We find that previous studies have substantially overestimated the performance of a 100 TeV proton-proton collider to measure the Higgs trilinear coupling. For a 3/ab data sample, we find a sensitivity to the trilinear coupling of order 30%, which is comparable to a measurement at the ILC. For a data set of 30/ab we find an  $\mathcal{O}(10\%)$  sensitivity subject to the details of background systematics.

This work is organised as follows: In Section II we review the kinematic Higgs distributions at 100 TeV, be-

fore presenting details of our analysis and simulations in Sec. III. In particular, we discuss  $hh \rightarrow b\bar{b}\gamma\gamma$  production in Sec. III A, and investigate  $hh + \text{jet}$  in Sec. III B. We present a combination of the results of these channels in Sec. III B, before we conclude with a brief discussion and comments on future studies in Sec. IV.

## II. KINEMATICS

We generate signal events at leading order in the Les Houches Event File format [27] using a combination of the VBFNLO [28] and FEYNARTS/FORMCALC/LOOPTOOLS [29] frameworks. We normalise to the NLO cross section by multiplying a phase-space independent  $K$ -factor of 1.65 [30, 31].

Our leading order results for  $\lambda = (0, 1, 2)\lambda_{\text{SM}}$  are  $\sigma_{\text{sig}} = (1676.9, 860.6, 415.5)$  fb respectively. These are to

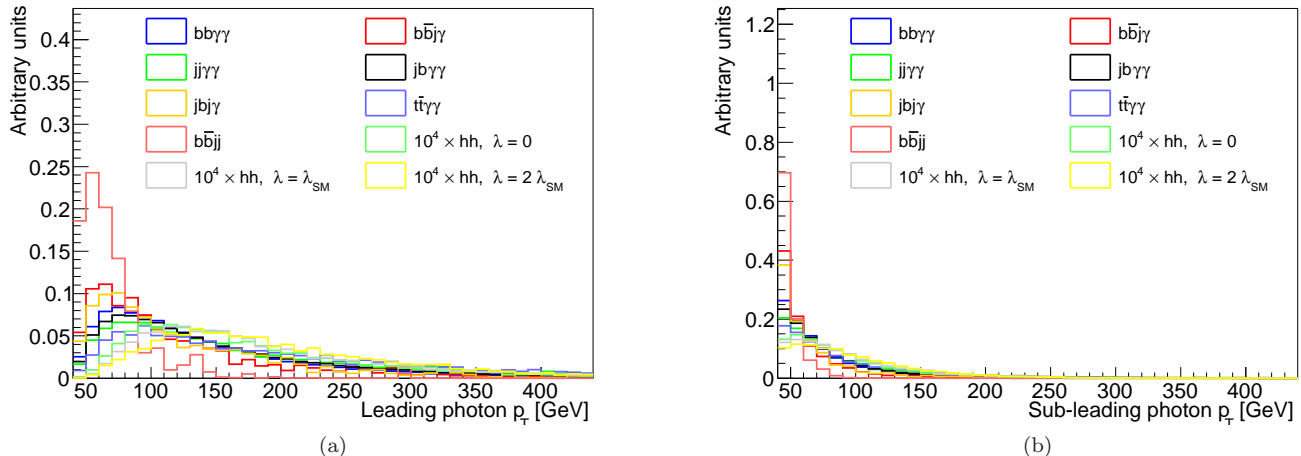


FIG. 3: The left panel (a) shows the transverse momentum of the leading photon in  $hh \rightarrow b\bar{b}\gamma\gamma$  events for  $\lambda = 0, \lambda_{\text{DM}}$  and  $2\lambda_{\text{SM}}$  along with various background contributions, while the right panel (b) shows the subleading photon transverse momentum.

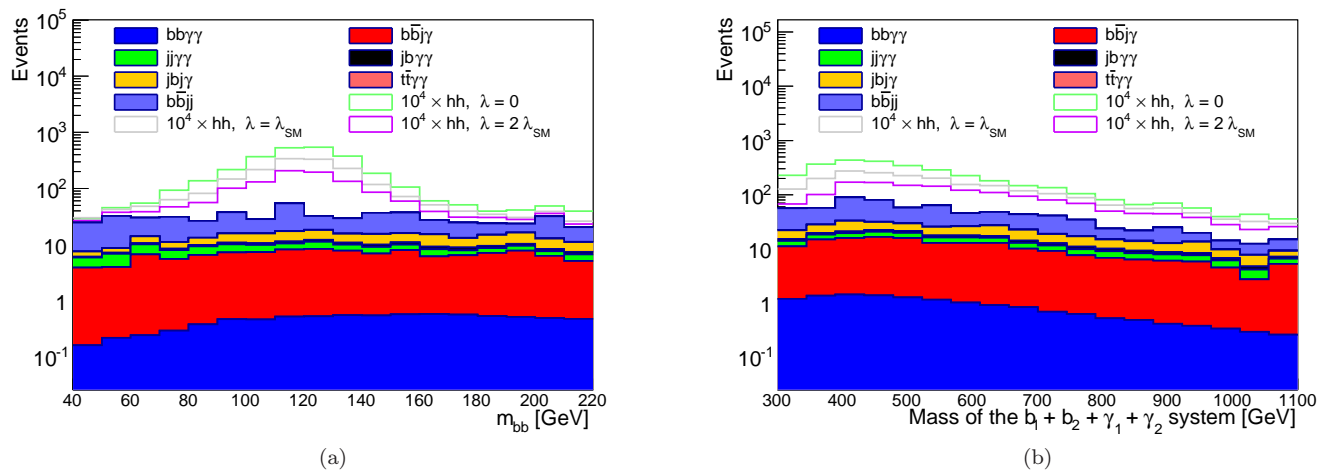


FIG. 4: The left panel (a) displays the differential  $m_{b\bar{b}}$  distribution for  $\lambda = 0, \lambda_{\text{DM}}$  and  $2\lambda_{\text{SM}}$  and background contributions. The right panel (b) shows the invariant mass of the 2-photon and 2- $b$ -jet system  $m_{b\bar{b}\gamma\gamma}$ .

be compared with an inclusive cross-section of 33.8 fb at NLO at 14 TeV for  $\lambda = \lambda_{\text{SM}}$  [31], an increase by a factor of  $\sim 40$ . To obtain the cross section after decays to photons and bottom quarks, we multiply with the branching ratio  $\text{Br}(hh \rightarrow b\bar{b}\gamma\gamma) \simeq 0.267\%$ .

In Fig. 1 we show the diHiggs invariant mass  $m_{hh}$  and Higgs  $p_T$  distributions at 100 TeV for  $\lambda = 0, \lambda_{\text{SM}}$  and  $2\lambda_{\text{SM}}$ , with the 14 TeV case for  $\lambda = \lambda_{\text{SM}}$  shown for comparison. While the 100 TeV distributions have considerably longer tails at high momentum and invariant mass, they are broadly similar to the 14 TeV ones. In particular, the peak in the  $m_{hh}$  spectrum at around 400 GeV and the peak in the partonic Higgs transverse momentum just near  $m_t$  due to the diHiggs system being produced near threshold. Due to the interference between the triangle and box diagrams the region around  $s \sim 4m_t^2$  is most sensitive to  $\lambda$ .

This relatively small invariant mass window which pro-

vides the most sensitive probe of  $\lambda$  asks for a selection as inclusive as possible. Such a selection is not possible in the  $b\bar{b}\tau\tau$  and  $b\bar{b}W^+W^-$  modes, as they crucially rely on the boosted kinematics regime. However, as demonstrated in [10], lower invariant diHiggs masses can be obtained by recoiling the diHiggs system against a hard jet. Such a process becomes increasingly likely when we increase the centre of mass energy as energetic jet radiation becomes unsuppressed. Indeed, as displayed in Fig. 2, the region of sensitivity to  $\lambda$  is reduced for recoils at  $p_{T,j} \geq 80$  GeV. However, the price to be paid is in smaller total cross sections which we compute at leading order to be (494.5, 262.9, 149.3) fb for  $\lambda = (0, 1, 2)\lambda_{\text{SM}}$  for jets with  $|\eta_j| < 4.5$ .

The Higgs bosons in very high energy diHiggs events are typically produced in the central pseudorapidity region. For the inclusive  $hh$  case it is important to stress that a considerable fraction of the cross section stems

from relatively small scattering angles at large pseudo-rapidity. Hence it is desirable to have as much forward detector coverage as possible to access these events at a 100 TeV collider.

### III. ANALYSIS

#### Event Generation and Detector Simulation

We generate the QCD and electroweak background events using MADGRAPH 5 [32], which are showered and hadronised with PYTHIA 8 [33]. Of particular importance in this channel are the so-called reducible backgrounds where jets can fake a hard photon. For all the backgrounds we use the leading order cross sections as obtained from MADEVENT. In our analysis for  $hh \rightarrow b\bar{b}\gamma\gamma$  we consider all reducible and irreducible backgrounds with at least four reconstructed objects in the final state without merging.

Because the irreducible and reducible backgrounds for this final state are large compared to the signal, we devote particular care to simulating fake rates. However, we stress that our parametrisation of fake rates and the detector response is based on the present performance of ATLAS and CMS and will likely deviate from that of an envisioned detector designed for  $\sqrt{s} = 100$  TeV.

When reconstructing the final state objects we consider all visible particles with  $|\eta| < 5.0$ . We smear the momenta of all reconstructed final state objects with Gaussians, using the parametrisations of [34] for jets and muons, as well as a 95% jet reconstruction efficiency, and we take the electron smearing parametrisation from [35]. The photons were smeared using a Gaussian with standard deviation of 0.1% of the photon  $p_T$ . We simulate  $b$ -tagging by matching a jet with a hadron containing a bottom or charm before decay and multiply a flat  $b$ -tagging efficiency of 70%, a mis-tag rate of 10% for  $c$ -jets and 1% for light-flavor jets. We assume the jet-faking-lepton and jet-faking-photon probabilities to be momentum-dependent and parametrise them to be  $\mathcal{P}_{j \rightarrow l} = 0.0048 \times e^{-0.035 p_{T,j}/\text{GeV}}$  and  $\mathcal{P}_{j \rightarrow \gamma} = 0.0093 \times e^{-0.036 p_{T,j}/\text{GeV}}$ , respectively. We further take into account jet, photon and muon detection efficiencies parametrised according to [34], while the electron efficiency is taken from [35]. We do not distinguish between the tagging rates in the barrel and endcaps.

The detector parametrisation used is very conservative, particularly on the photon identification efficiency, which is parametrised as  $\mathcal{E}_\gamma = 0.76 - 1.98 e^{-p_{T,\gamma}/16.1 \text{ GeV}}$ . This efficiency performance has a turn on curve that only reaches a  $> 70\%$  efficiency at  $\sim 60$  GeV, while for a 20 GeV photon, its detection efficiency is only 18%. This is a significant limitation on the analysis, as the photons from the Higgs decay are expected to have often a lower  $p_T$ , as can be seen in Fig. 3. The results can be improved if one is allowed to reduce the photon  $b$ -jet transverse momentum thresholds in 100 TeV machine,

with turn on curve reaching a stable efficiency at a lower transverse momentum. This would increase the signal acceptance in the analysis, and it would open space for more elaborate techniques for background rejection.

#### A. $hh \rightarrow b\bar{b}\gamma\gamma$

To reconstruct the  $b\bar{b}\gamma\gamma$  final state we require two reconstructed anti- $k_T$  jets with  $R = 0.4$  and  $p_T > 40$  GeV within  $|\eta| < 3.0$ . The jets are recombined using FASTJET [36]. For the photons we require  $p_T > 40$  GeV and  $|\eta| < 3.0$ . To ensure the photons are isolated we sum the energy of the visible particles in a cone of  $R = 0.3$  around the photon and we only accept them if  $p_{T,\text{vis}}/p_{T,\gamma} \leq 0.05$ . Likewise, we reject a jet if  $\Delta R_{\text{jet},\gamma} < 0.3$  for any jet- $\gamma$  combination and for  $\Delta R_{\gamma,\gamma} < 0.4$  we reject the softer photon. For both the jets and photons we smear the four-momenta of the reconstructed objects as mentioned in the previous section.

To identify isolated leptons with  $p_T > 40$  GeV we apply the same isolation requirement as for the photons. To accept an event we require two  $b$ -jets and two photons. Events with one or more isolated leptons are vetoed. At this stage of the analysis we find a small signal-over-background ratio of  $S/B \simeq 3 \times 10^{-4}$  and  $S/\sqrt{B} \simeq 0.28$  after 3000/fb.

To enhance  $S/B$  we apply cuts on the maximum angular separation and the vectorial sum of the transverse momentum of the two hardest photons and  $b$ -jets respectively (see Tab. II for a detailed cut flow). In particular we require  $\Delta R_{b_1,b_2} < 1.7$ ,  $\Delta R_{\gamma_1,\gamma_2} < 1.7$ ,  $p_{T,b\bar{b}} > 150$  GeV and  $p_{T,\gamma\gamma} > 150$  GeV. As a next step, a selection requirement on the  $\phi$  difference between the sub-leading  $b$ -jet and the two hardest photons is required to be greater than 1.6. After applying these kinematic cuts we find  $S/B \simeq 3 \times 10^{-3}$  and  $S/\sqrt{B} \simeq 0.9$ .

Finally the  $b$ -jets and photons are recombined to the Higgs mass with  $|m_{b\bar{b}} - 120| < 30$  GeV and  $|m_{\gamma\gamma} - 125| < 1$  GeV. The narrow window for the invariant mass of the di-photon system allows the rejection of a large fraction of the backgrounds and improves the statistical significance of the analysis to  $S/B \simeq 0.4$  and  $S/\sqrt{B} \simeq 8.45$  for  $\lambda = \lambda_{\text{SM}}$ .

Compared to the ATLAS analysis in [37], the transverse momentum requirement for the photons and  $b$ -jets is required to be stricter in an attempt to control the effect of the pile up contribution, while otherwise the pre-selection is made in a very similar way, including the veto on isolated leptons. While no pile up jets were added or simulated, the parametrisation used for the objects' reconstruction and identification include the effect of the pile up in the detector performance.

The parametrisation used in this study for the detector is similar to the one used in the [37]. Two exceptions are the  $b$ -tagging performance, which was taken as a constant and not depending on the transverse momentum, and the Gaussian smearing functions for the photons have a

Sample	$\Delta R(b_1, b_2)$	$\Delta R(\gamma_1, \gamma_2)$	$p_{T,\gamma\gamma}$	$p_{T,bb}$	$\Delta\phi(b_2, \gamma\gamma)$	$m_{bb}$	$m_{\gamma\gamma}$
$(h \rightarrow bb)(h \rightarrow \gamma\gamma)\lambda = \lambda_{SM}$	$1.18 \times 10^{-1}$	$1.05 \times 10^{-1}$	$9.76 \times 10^{-2}$	$8.40 \times 10^{-2}$	$6.85 \times 10^{-2}$	$5.96 \times 10^{-2}$	$5.96 \times 10^{-2}$
$(h \rightarrow b\bar{b})(h \rightarrow \gamma\gamma)\lambda = 0$	$1.93 \times 10^{-1}$	$1.68 \times 10^{-1}$	$1.54 \times 10^{-1}$	$1.29 \times 10^{-1}$	$1.03 \times 10^{-1}$	$8.88 \times 10^{-2}$	$8.87 \times 10^{-2}$
$(h \rightarrow b\bar{b})(h \rightarrow \gamma\gamma)\lambda = 2\lambda_{SM}$	$6.74 \times 10^{-2}$	$6.24 \times 10^{-2}$	$5.95 \times 10^{-2}$	$5.30 \times 10^{-2}$	$4.55 \times 10^{-2}$	$3.91 \times 10^{-2}$	$3.91 \times 10^{-2}$
$jj\gamma\gamma$	$2.76 \times 10^1$	8.94	5.99	4.46	3.88	1.48	$7.20 \times 10^{-2}$
$bbj\gamma$	$5.97 \times 10^1$	$2.01 \times 10^1$	$1.08 \times 10^1$	8.75	8.18	3.04	$1.43 \times 10^{-2}$
$b\bar{b}jj$	$1.99 \times 10^2$	$4.79 \times 10^1$	$1.47 \times 10^1$	7.82	7.67	$2.81 \times 10^{-1}$	$5.06 \times 10^{-3}$
$t\bar{t}\gamma\gamma$	1.01	$4.31 \times 10^{-1}$	$3.62 \times 10^{-1}$	$2.78 \times 10^{-1}$	$2.22 \times 10^{-1}$	$9.06 \times 10^{-2}$	$3.38 \times 10^{-2}$
$b\bar{b}\gamma\gamma$	2.70	$8.26 \times 10^{-1}$	$5.80 \times 10^{-1}$	$4.58 \times 10^{-1}$	$4.48 \times 10^{-1}$	$1.69 \times 10^{-1}$	$1.21 \times 10^{-2}$
$jbj\gamma$	$3.61 \times 10^1$	8.37	5.70	4.34	3.88	$7.24 \times 10^{-1}$	$3.04 \times 10^{-3}$
$jb\gamma\gamma$	5.18	1.57	$9.86 \times 10^{-1}$	$7.91 \times 10^{-1}$	$6.99 \times 10^{-1}$	$2.41 \times 10^{-1}$	$8.57 \times 10^{-3}$
Background	$3.31 \times 10^2$	$8.81 \times 10^1$	$3.91 \times 10^1$	$2.69 \times 10^1$	$2.50 \times 10^1$	6.03	$1.49 \times 10^{-1}$
$S/B (\lambda/\lambda_{SM} = 0)$	0.00058	0.0019	0.0039	0.0048	0.0041	0.015	0.59
$S/\sqrt{B} (\lambda/\lambda_{SM} = 0)$	0.58	0.98	1.35	1.36	1.13	1.98	12.58
$S/B (\lambda/\lambda_{SM} = 1)$	0.00036	0.0012	0.0025	0.0031	0.0027	0.0099	0.4
$S/\sqrt{B} (\lambda/\lambda_{SM} = 1)$	0.36	0.62	0.85	0.89	0.75	1.33	8.45
$S/B (\lambda/\lambda_{SM} = 2)$	0.0002	0.00071	0.0015	0.002	0.0018	0.0065	0.26
$S/\sqrt{B} (\lambda/\lambda_{SM} = 2)$	0.20	0.36	0.52	0.56	0.50	0.87	5.54

TABLE I: This table shows the cutflow and cross-sections for the  $b\bar{b}\gamma\gamma$  analysis. The cross sections are given in femtobarns, and  $S/\sqrt{B}$  is shown for a luminosity of 3000/fb. After the pre-selection described on the text, the  $\Delta R$  between the two leading  $b$ -jets and the two leading photons is required to be  $< 1.7$ , and the cross section after this selection is shown in the second and third columns. The transverse momentum of the 2-photons and 2- $b$ -jets systems are required to be  $> 150$  GeV, as shown in the fourth and fifth columns. The  $\Delta\phi$  between the sub-leading  $b$ -jet and the diphoton system is required to be  $\Delta\phi > 1.6$ . Finally the cuts on the invariant mass of the two hardest  $b$ -jets and photons are implemented as  $|m_{bb} - 120 \text{ GeV}| < 30 \text{ GeV}$  and  $|m_{\gamma\gamma} - 125 \text{ GeV}| < 1 \text{ GeV}$ . Further details on the cuts can be found in the text.

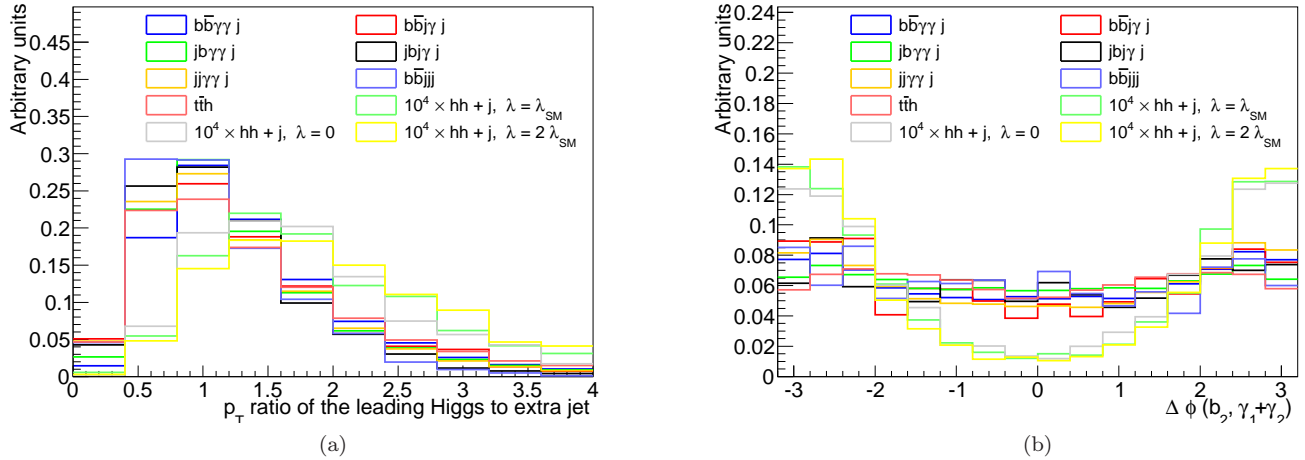


FIG. 5: The left panel (a) shows the ratio of the transverse momentum of leading reconstructed Higgs to the transverse momentum of the extra jet for  $\lambda = 0, \lambda_{SM}$  and  $2\lambda_{SM}$  as well as the backgrounds. The right panel (b) shows the  $\Delta\phi$  between the subleading  $b$ -jet and the  $\gamma\gamma$  system for the same data.

$0.1\% \times p_T$  standard deviation in our study. The  $\Delta R$  requirements on the hardest  $b$ -jets and photons were also taken to be stricter (1.6 as opposed to 2.0 in the ATLAS note), although the overlap removal selection is implemented similarly. The mass selection used in this article is also stricter for the two photon system, using a 2 GeV window, while the ATLAS note uses a 5 GeV window

instead. The mass selection on the two  $b$ -jet system is, however, stricter in the ATLAS note than in this document, as a 60 GeV window is used here, while the ATLAS note uses a 50 GeV window. Finally, the transverse momentum of the two  $b$ -jets and of the two hardest photons have a stricter selection in this article (150 GeV), compared to the ATLAS one (110 GeV). We also use a  $\Delta\phi$



Sample	Pre-selected	$N_{jets} \geq 3$	Extra jet $p_T$	$p_{T,\gamma\gamma}$	$m_{bb}$	$m_{\gamma\gamma}$	$N_{jets} \leq 6$	$\Delta\phi(b_2, \gamma\gamma)$	$p_{T,h1}/p_{T,j}$
$hh(bb\gamma\gamma) + j, \lambda = 0$	$5.85 \times 10^{-2}$	$4.98 \times 10^{-2}$	$3.57 \times 10^{-2}$	$3.10 \times 10^{-2}$	$2.23 \times 10^{-2}$	$2.22 \times 10^{-2}$	$2.16 \times 10^{-2}$	$1.76 \times 10^{-2}$	$1.61 \times 10^{-2}$
$hh(b\bar{b}\gamma\gamma) + j, \lambda/\lambda_{SM} = 1$	$3.56 \times 10^{-2}$	$3.08 \times 10^{-2}$	$2.18 \times 10^{-2}$	$1.91 \times 10^{-2}$	$1.36 \times 10^{-2}$	$1.35 \times 10^{-2}$	$1.32 \times 10^{-2}$	$1.13 \times 10^{-2}$	$1.06 \times 10^{-2}$
$hh(bb\gamma\gamma) + j, \lambda/\lambda_{SM} = 2$	$2.09 \times 10^{-2}$	$1.85 \times 10^{-2}$	$1.33 \times 10^{-2}$	$1.21 \times 10^{-2}$	$8.50 \times 10^{-3}$	$8.49 \times 10^{-3}$	$8.30 \times 10^{-3}$	$7.20 \times 10^{-3}$	$6.91 \times 10^{-3}$
$bb\gamma\gamma j$ (QED=2)	7.62	6.74	5.21	2.83	$4.39 \times 10^{-1}$	$2.48 \times 10^{-3}$	$2.48 \times 10^{-3}$	$2.04 \times 10^{-3}$	$1.75 \times 10^{-3}$
$b\bar{b}\gamma\gamma j$ (QED=4)	$1.39 \times 10^{-1}$	$1.25 \times 10^{-1}$	$9.80 \times 10^{-2}$	$6.05 \times 10^{-2}$	$2.56 \times 10^{-2}$	$9.32 \times 10^{-5}$	$9.32 \times 10^{-5}$	$7.96 \times 10^{-5}$	$7.96 \times 10^{-5}$
$t\bar{t}h(\rightarrow \gamma\gamma)$	$7.34 \times 10^{-1}$	$6.91 \times 10^{-1}$	$5.32 \times 10^{-1}$	$4.02 \times 10^{-1}$	$4.44 \times 10^{-2}$	$4.39 \times 10^{-2}$	$3.76 \times 10^{-2}$	$2.55 \times 10^{-2}$	$2.03 \times 10^{-2}$
$jj\gamma\gamma j$	$1.66 \times 10^1$	$1.55 \times 10^1$	$1.26 \times 10^1$	7.87	1.46	$7.10 \times 10^{-3}$	$6.95 \times 10^{-3}$	$4.58 \times 10^{-3}$	$4.41 \times 10^{-3}$
$b\bar{b}j\gamma j$	$4.84 \times 10^1$	$4.48 \times 10^1$	$3.55 \times 10^1$	$1.88 \times 10^1$	3.25	$8.51 \times 10^{-2}$	$8.49 \times 10^{-2}$	$1.46 \times 10^{-3}$	$1.17 \times 10^{-3}$
$jb\gamma\gamma j$	5.20	4.76	3.75	2.15	$2.02 \times 10^{-1}$	$1.52 \times 10^{-3}$	$1.52 \times 10^{-3}$	$8.67 \times 10^{-4}$	$6.88 \times 10^{-4}$
$jbj\gamma j$	$1.65 \times 10^1$	$1.57 \times 10^1$	$1.29 \times 10^1$	6.55	$4.58 \times 10^{-1}$	$1.25 \times 10^{-3}$	$1.24 \times 10^{-3}$	$8.75 \times 10^{-4}$	$5.97 \times 10^{-4}$
$b\bar{b}jjj$	$3.10 \times 10^1$	$2.93 \times 10^1$	$2.23 \times 10^1$	4.52	$7.54 \times 10^{-1}$	$1.30 \times 10^{-3}$	$1.06 \times 10^{-3}$	$7.29 \times 10^{-4}$	$2.44 \times 10^{-4}$
Background	$1.26 \times 10^2$	$1.18 \times 10^2$	$9.28 \times 10^1$	$4.32 \times 10^1$	6.64	$1.43 \times 10^{-1}$	$1.36 \times 10^{-1}$	$3.61 \times 10^{-2}$	$2.93 \times 10^{-2}$
$S/B$ ( $\lambda/\lambda_{SM} = 0$ )	0.00046	0.00042	0.00038	0.00072	0.0034	0.16	0.16	0.49	0.55
$S/\sqrt{B}$ ( $\lambda/\lambda_{SM} = 0$ )	0.29	0.25	0.20	0.26	0.47	3.22	3.21	5.08	5.17
$S/B$ ( $\lambda/\lambda_{SM} = 1$ )	0.00028	0.00026	0.00023	0.00044	0.002	0.095	0.097	0.31	0.36
$S/\sqrt{B}$ ( $\lambda/\lambda_{SM} = 1$ )	0.17	0.16	0.12	0.16	0.29	1.96	1.96	3.26	3.39
$S/B$ ( $\lambda/\lambda_{SM} = 2$ )	0.00017	0.00016	0.00014	0.00028	0.0013	0.059	0.061	0.2	0.24
$S/\sqrt{B}$ ( $\lambda/\lambda_{SM} = 2$ )	0.10	0.09	0.08	0.10	0.18	1.23	1.23	2.08	2.21

TABLE II: This table shows the cutflow for the  $hh + j$  analysis. The cross sections are given in femtobarn, and  $S/\sqrt{B}$  is shown for a luminosity of 3000/fb. After the pre-selection described in the text, a jet multiplicity requirement is implemented to guarantee there is one extra jet besides the two Higgs  $b$ -jets and the cross section after this requirement is shown in the third column. The transverse momentum of the extra jet is required to be greater than 100 GeV in the following column. The transverse momentum of the two hardest photons is required to be greater than 160 GeV in the fifth column, and is followed by the Higgs mass requirements of  $|m_{bb} - 120 \text{ GeV}| < 30 \text{ GeV}$  and  $|m_{\gamma\gamma} - 125 \text{ GeV}| < 1 \text{ GeV}$ . The  $t\bar{t}h$  background is reduced by the jet multiplicity requirement that there are  $\leq 6$  jets in the eighth column. The  $\Delta\phi$  selection between the subleading  $b$ -jet and the hardest two photons system is required to be greater than 1.6 in the next column. Finally the transverse momentum ratio between the leading reconstructed Higgs and the extra jet is required to be greater than 1. Further details on the cuts can be found in the text.

selection to reduce the impact of the backgrounds.

### B. $hh + \text{jet} \rightarrow \bar{b}b\gamma\gamma + \text{jet}$

The majority of sensitivity to variations of the Higgs trilinear coupling arises when the triangle diagram is resonantly enhanced. Unfortunately, experimental selection cuts often select regions of phase space far away from this regime (this is particularly true of boosted analyses). However, this fact can be mitigated by producing the diHiggs system at resonance in opposition to a high  $p_T$  recoiling ISR jet [10]. In this section we therefore consider the sensitivity such an analysis would have at a 100 TeV hadron collider.

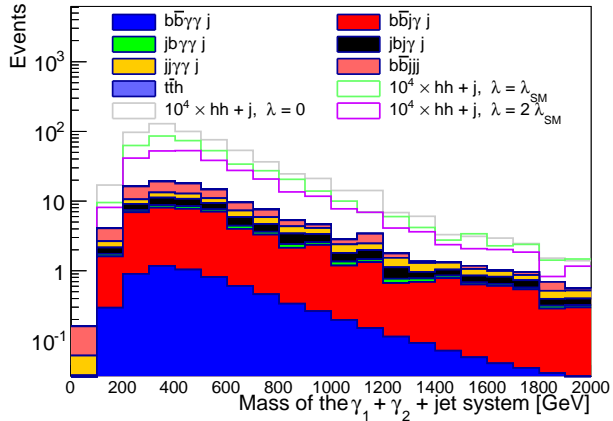
The pre-selection in this study uses a higher jet transverse momentum and photon selection (50 GeV) and more restricted range of rapidities ( $|\eta| < 2.4$ ) than the pre-selection cuts than the previous section. The remaining pre-selection cuts are unchanged. However, the event selection has been optimised for this particular topology by demanding at least three jets and that the extra jet produced with the  $hh$  system has  $p_T \geq 100 \text{ GeV}$ . The two leading  $b$ -jets are used as the jets from the Higgs decay. The extra jet is chosen such that it is not one of the  $b$ -jets used for the Higgs reconstruction and that it is the highest transverse momentum jet choice. A further selection is applied on the transverse momentum of the  $\gamma\gamma$  system, which is required to be greater than 160 GeV.

Similar to the analysis in the previous section, the

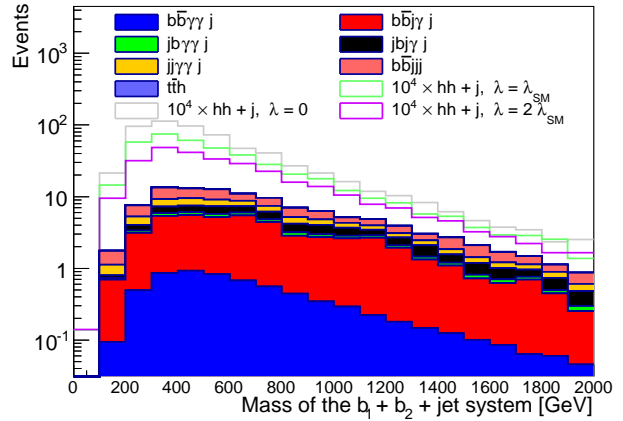
Higgs mass requirements are applied such that  $m_{bb} \in [90, 150] \text{ GeV}$  and  $m_{\gamma\gamma} \in [124, 126] \text{ GeV}$ . In this final state the impact of the  $t\bar{t}h$  background is significant, as the signal already has extra high transverse momentum jets. To veto the impact of this background, an upper bound is implemented on the jet multiplicity,  $N_{jets} \leq 6$ . The signal-over-background ratio is also slightly increased by a requirement on the  $\Delta\phi$  between the subleading  $b$ -jet and the  $\gamma\gamma$  system, such that  $\Delta\phi(b_2, \gamma\gamma) > 1.6$ , which can be seen to improve the discrimination, as seen in Fig. 5 (b).

The final selection criterion applied is on the ratio of the transverse momentum of the leading reconstructed Higgs and the transverse momentum of the extra jet, which is required to be greater than one, reducing some backgrounds as can be seen in Fig. 5 (a). The invariant masses of the  $\gamma\gamma$  and the extra jets, the 2  $b$ -jets and the extra jet and the  $b\bar{b}\gamma\gamma j$  system are shown in Fig. 6 panels (a), (b) and (c).

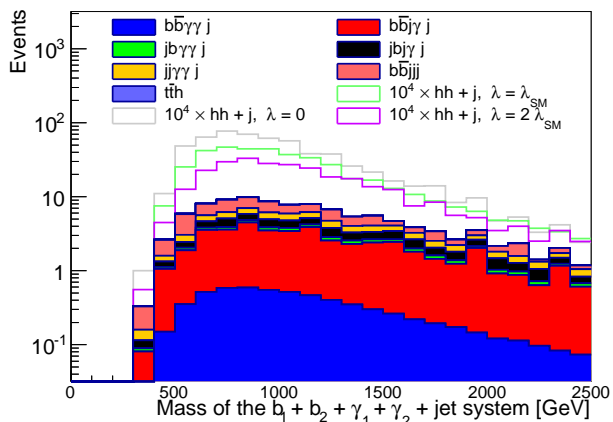
One important limitation is the high value of the minimum jet  $p_T$ , aimed at avoiding pile up contamination and rejecting QCD backgrounds. Signal events are rejected not only for failing the minimum jet multiplicity requirement, but because one of the Higgs  $b$ -jets may fail this selection criterion. This jet selection removes 59% of the signal after demanding at least 2 jets only, while it also has the side effect of rejecting an extra 50% of the events which fail the  $b$ -tagging selection when one of the  $b$ -jets is rejected. The sensitivity of the analysis could be improved with lower transverse momentum selection if a



(a)



(b)



(c)

FIG. 6: Panel (a) shows the invariant mass distribution of the two hardest isolated photons and the extra jet  $m_{\gamma\gamma j}$  for the  $hh + \text{jet}$  analysis. Panel (b) displays  $m_{b\bar{b}j}$  and panel (c) shows the invariant mass of the 2-photon, 2- $b$ -jet and extra jet system  $m_{b\bar{b}\gamma\gamma j}$ . We show the signal distributions for  $\lambda = 0, \lambda_{\text{SM}}$  and  $2\lambda_{\text{SM}}$  and the backgrounds in all cases.

better photon identification performance at low energies becomes possible in the future.

## Results

We now combine both analyses in the  $b\bar{b}\gamma\gamma$  channel to formulate a constraint on the Higgs trilinear coupling in light of the expected signal and background yields in  $pp \rightarrow hh + X$  and  $pp \rightarrow hh + \text{jet} + X$  production. For simplicity we assume that both measurements are statistically uncorrelated and combine them in a binned log-likelihood hypothesis test [38, 39]. We compute a 95% confidence level using the CLS method [40] around the SM parameter choice  $\lambda = \lambda_{\text{SM}}$  and find

$$\frac{\lambda}{\lambda_{\text{SM}}} \in \begin{cases} [0.672, 1.406] & \text{no background syst.} \\ [0.646, 1.440] & 25\% hh, 25\% hh + \text{jet} \\ [0.642, 1.448] & 25\% hh, 50\% hh + \text{jet} \end{cases} \quad (3)$$

for an integrated luminosity of 3000/fb. Due to the shape of the cross section as a function of  $\lambda$ , there is a parameter choice at  $\lambda \simeq 4\lambda_{\text{SM}}$  with SM-like cross sections.

This region can be excluded using the high luminosity phase of the 14 TeV LHC [15].

In the calculation of the confidence level intervals the quoted systematic uncertainties refer to a flat rescaling of the contributing backgrounds. From Eq. (3) we can expect that a measurement of the trilinear coupling at the 40% level should be possible. A  $5\sigma$  discovery of the diHiggs signal will be possible with an integrated luminosity of 700/fb.

A number of authors have noted that a total integrated luminosity of 3/ab may not be sufficient to saturate the physics potential of a 100 TeV collider [41, 42], since the necessary luminosity typically scales quadratically with the centre of mass energy. We therefore also compute limits under the assumption that 30/ab of data is taken. The limits shown in Eq. (3) then improve to

$$\frac{\lambda}{\lambda_{\text{SM}}} \in \begin{cases} [0.891, 1.115] & \text{no background syst.} \\ [0.882, 1.126] & 25\% hh, 25\% hh + \text{jet} \\ [0.881, 1.128] & 25\% hh, 50\% hh + \text{jet} \end{cases} \quad (4)$$

in this case. We note that these limits are nearly identical to what can be achieved with the 1 TeV luminosity upgraded ILC.

We note that that the theoretical uncertainty on the  $hh$  signal was not taken into account in the limit setting. Although the signal theoretical uncertainty is estimated to be large currently, mainly due to the fact that full high order calculations are unavailable, the 100 TeV machine is relatively far in the future. It is expected this theoretical uncertainty will be reduced in the future.

Most of the statistical pull in the  $b\bar{b}\gamma\gamma$  channel results from  $pp \rightarrow hh + X$  production. This is expected from our discussion in the previous section and is likely to change in other final states such as  $b\bar{b}\tau\tau$  [10, 11].

#### IV. DISCUSSION AND CONCLUSIONS

The precision measurement of the Higgs trilinear coupling at a future high energy hadron collider is an important motivation for the construction of such a machine. In this paper we have performed an analysis of diHiggs final states in the  $b\bar{b}\gamma\gamma$  channel at a 100 TeV hadron collider. In particular, we have explored to what extent additional hard jet emission contributes extra statistical discriminative power. In doing so we have implemented realistic estimates for the final state reconstruction and arrive at the conclusion that a measurement at 40% level can be expected at 3/ab, which improves to the 10% with a factor 10 larger data set of 30/ab.

Comparing to earlier analyses performed as part of the Snowmass process [19], we find a significantly smaller sensitivity, which results from the more realistic treatment of backgrounds, expected detector resolution effects, pile up and, most importantly, fake rates.

The limiting factor of the  $b\bar{b}\gamma\gamma$  channels is the size of reducible backgrounds for an acceptably large signal yield. While in this initial study we focus on the  $b\bar{b}\gamma\gamma$  final state, it would hence be interesting to extend this study to other final states, and look at the use of taggers in the  $b\bar{b}\tau\tau$  or  $b\bar{b}WW$  final states, which, due to bigger signal cross sections, opens more opportunities to exploit the high invariant mass distributions and the  $hh + \text{jet}$  final state [10].

We would like to point out that another study on the  $hh \rightarrow b\bar{b}\gamma\gamma$  has recently appeared in [43].

#### Acknowledgments

CE is supported by the Institute for Particle Physics Phenomenology Associateship programme. This research was supported in part by the European Commission through the HiggsTools Initial Training Network PITN-GA-2012-316704. AJB gratefully acknowledges the support of UK Science and Technology Facilities Council, the IPPP (Durham), and Merton College, Oxford.

- 
- [1] F. Englert and R. Brout, Phys. Rev. Lett. **13** (1964) 321; P. W. Higgs, Phys. Lett. **12** (1964) 132 and Phys. Rev. Lett. **13** (1964) 508; G. S. Guralnik, C. R. Hagen and T. W. B. Kibble, Phys. Rev. Lett. **13** (1964) 585.
- [2] G. Aad *et al.* [ATLAS Collaboration], Phys. Lett. B **716** (2012) 1; S. Chatrchyan *et al.* [CMS Collaboration], Phys. Lett. B **716** (2012) 30.
- [3] S. Chatrchyan *et al.* [CMS Collaboration], JHEP **06** (2013) 081; G. Aad *et al.* [ATLAS Collaboration], arXiv:1307.1427 [hep-ex].
- [4] R. Grober and M. Mühlleitner, JHEP **1106** (2011) 020; R. Contino, M. Ghezzi, M. Moretti, G. Panico, F. Piccinini and A. Wulzer, JHEP **1208** (2012) 154; M. Gillioz, R. Grober, C. Grojean, M. Mühlleitner and E. Salvioni, JHEP **1210** (2012) 004.
- [5] M. J. Dolan, C. Englert and M. Spannowsky, Phys. Rev. D **87** (2013) 055002.
- [6] F. Goertz, A. Papaefstathiou, L. L. Yang and J. Zurita, arXiv:1410.3471 [hep-ph].
- [7] T. Plehn and M. Rauch, Phys. Rev. D **72** (2005) 053008.
- [8] E. W. N. Glover and J. J. van der Bij, Nucl. Phys. B **309** (1988) 282; D. A. Dicus, C. Kao and S. S. D. Willenbrock, Phys. Lett. B **203** (1988) 457; A. Djouadi, W. Kilian, M. Mühlleitner and P. M. Zerwas, Eur. Phys. J. C **10** (1999) 45.
- [9] U. Baur, T. Plehn and D. L. Rainwater, Phys. Rev. D **68** (2003) 033001.
- [10] M. J. Dolan, C. Englert and M. Spannowsky, JHEP **1210** (2012) 112.
- [11] A. J. Barr, M. J. Dolan, C. Englert and M. Spannowsky, Phys. Lett. B **728** (2014) 308.
- [12] A. Papaefstathiou, L. L. Yang and J. Zurita, Phys. Rev. D **87** (2013) 011301.
- [13] D. E. Ferreira de Lima, A. Papaefstathiou and M. Spannowsky, JHEP **1408** (2014) 030.
- [14] M. J. Dolan, C. Englert, N. Greiner and M. Spannowsky, Phys. Rev. Lett. **112** (2014) 101802.
- [15] C. Englert, F. Krauss, M. Spannowsky and J. Thompson, arXiv:1409.8074 [hep-ph].
- [16] T. Liu and H. Zhang, arXiv:1410.1855 [hep-ph].
- [17] T. Plehn, M. Spira and P. M. Zerwas, Nucl. Phys. B **479** (1996) 46 [Erratum-ibid. B **531** (1998) 655]; U. Baur, T. Plehn and D. L. Rainwater, Phys. Rev. Lett. **89** (2002) 151801. U. Baur, T. Plehn and D. L. Rainwater, Phys. Rev. D **67**, 033003 (2003). U. Baur, T. Plehn and D. L. Rainwater, Phys. Rev. D **69** (2004) 053004.
- [18] V. Barger, L. L. Everett, C. B. Jackson and G. Shaughnessy, Phys. Lett. B **728** (2014) 433.
- [19] W. Yao, arXiv:1308.6302 [hep-ph].
- [20] The ATLAS Collaboration, ATL-PHYS-PUB-2014-019
- [21] Aram Apyan, Talk at ECFA HL-LHC Workshop 2014
- [22] F. Goertz, A. Papaefstathiou, L. L. Yang and J. Zurita, JHEP **1306** (2013) 016.
- [23] C. Durig, K. Fujii, J. List and J. Tian, arXiv:1403.7734 [hep-ex]; J. Tian *et al.* [ILD Collaboration], PoS EPS **-HEP2013**, 316 (2013); D. M. Asner, T. Barklow, C. Calanhan, K. Fujii, N. Graf, H. E. Haber, A. Ishikawa and S. Kanemura *et al.*, arXiv:1310.0763 [hep-ph]; M. McCullough, Phys. Rev. D **90** (2014) 015001.
- [24] S. Dawson, A. Gritsan, H. Logan, J. Qian, C. Tully,



- R. Van Kooten, A. Ajaib and A. Anastassov *et al.*, arXiv:1310.8361 [hep-ex].
- [25] R. S. Gupta, H. Rzehak and J. D. Wells, Phys. Rev. D **88** (2013) 055024.
- [26] T. Cohen, T. Golling, M. Hance, A. Henrichs, K. Howe, J. Loyal, S. Padhi and J. G. Wacker, JHEP **1404** (2014) 117; A. Fowlie and M. Raidal, Eur. Phys. J. C **74** (2014) 2948; T. G. Rizzo, Phys. Rev. D **89** (2014) 095022; M. Low and L. T. Wang, JHEP **1408** (2014) 161; A. Hook and A. Katz, JHEP **1409** (2014) 175; C. Borschensky, M. Krmer, A. Kulesza, M. Mangano, S. Padhi, T. Plehn and X. Portell, Eur. Phys. J. C **74** (2014) 12, 3174; B. S. Acharya, K. Bozek, C. Pongkitivanichkul and K. Sakurai, arXiv:1410.1532 [hep-ph]. S. Gori, S. Jung, L. T. Wang and J. D. Wells, arXiv:1410.6287 [hep-ph]. J. Bramante, P. J. Fox, A. Martin, B. Ostdiek, T. Plehn, T. Schell and M. Takeuchi, arXiv:1412.4789 [hep-ph].
- [27] E. Boos, M. Dobbs, W. Giele, I. Hinchliffe, J. Huston, V. Ilyin, J. Kanzaki and K. Kato *et al.*, hep-ph/0109068.
- [28] K. Arnold, M. Bahr, G. Bozzi, F. Campanario, C. Englert, T. Figy, N. Greiner and C. Hackstein *et al.*, Comput. Phys. Commun. **180** (2009) 1661.
- [29] T. Hahn, Comput. Phys. Commun. **140** (2001) 418; T. Hahn and M. Perez-Victoria, Comput. Phys. Commun. **118**, 153 (1999).
- [30] S. Dawson, S. Dittmaier and M. Spira, Phys. Rev. D **58** (1998) 115012.
- [31] J. Baglio, A. Djouadi, R. Grber, M. M. Hlleitner, J. Quevillon and M. Spira, JHEP **1304** (2013) 151; F. Maltoni, E. Vryonidou and M. Zaro, arXiv:1408.6542 [hep-ph].
- [32] J. Alwall, M. Herquet, F. Maltoni, O. Mattelaer and T. Stelzer, JHEP **1106** (2011) 128.
- [33] T. Sjostrand, S. Mrenna and P. Z. Skands, Comput. Phys. Commun. **178** (2008) 852.
- [34] The ATLAS Collaboration, “Performance assumptions based on full simulation for an upgraded ATLAS detector at a High-Luminosity LHC,” ATLAS PUB note ATL-PHYS-PUB-2013-009, Sep 2013.
- [35] The ATLAS Collaboration, “Performance assumptions for an upgraded ATLAS detector at a High-Luminosity LHC,” ATLAS PUB note ATL-PHYS-PUB-2013-004, Mar 2013.
- [36] M. Cacciari, G. P. Salam and G. Soyez, Eur. Phys. J. C **72** (2012) 1896.
- [37] The ATLAS Collaboration, “Prospects for measuring Higgs pair production in the channel  $H(\rightarrow \gamma\gamma)H(\rightarrow b\bar{b})$  using the ATLAS detector at the HL-LHC,” ATLAS PUB note ATL-PHYS-PUB-2014-019, Oct 2014.
- [38] A. W. F. Edwards, “Likelihoods”, Cambridge University Press, 1972.
- [39] T. Junk, Nucl. Instrum. Meth. A **434** (1999) 435; T. Junk, CDF Note 8128 [cdf/doc/statistics/public/8128]; T. Junk, CDF Note 7904 [cdf/doc/statistics/public/7904].
- [40] A. L. Read, CERN-OPEN-2000-205; A. L. Read, J. Phys. G **G28** (2002) 2693-2704.
- [41] T. Cohen, R. T. D’Agnolo, M. Hance, H. K. Lou and J. G. Wacker, JHEP **1411** (2014) 021.
- [42] B. Richter, arXiv:1409.1196 [hep-ex].
- [43] A. Azatov, R. Contino, G. Panico and M. Son, arXiv:1502.00539 [hep-ph].

